



Cite this: *Dalton Trans.*, 2015, **44**, 9470

New donor–acceptor conjugates based on a trifluorenylporphyrin linked to a redox–switchable ruthenium unit†‡

Areej Merhi,^{a,b} Xu Zhang,^{a,b} Dandan Yao,^{a,b} Samuel Drouet,^a Olivier Mongin,^a Frédéric Paul,^a J. A. Gareth Williams,^c Mark A. Fox^{*c} and Christine O. Paul-Roth^{*a,b}

Reactions of the 16-electron ruthenium complex $[\text{Ru}(\text{dppe})_2\text{Cl}][\text{PF}_6]$ with metal-free and zinc ethynylphenyltrifluorenylporphyrins **1** and **2** respectively, gave the new dyads **3** and **4** with ethynylruthenium group as a potential electron donor and the porphyrin as a potential electron acceptor. The redox properties of the porphyrins **1–4** were investigated by cyclic voltammetry and UV spectroelectrochemistry (SEC), which reveal that the monocation and monoanion of metal-free porphyrin **1** are stable under these conditions whereas the formation of the corresponding radical cation or anion of the zinc porphyrin **2** was accompanied by partial decomplexation of the zinc ion. Oxidations of the dyads **3** and **4** gave stable radical cations as probed using IR, NIR and UV SEC methods. These cations show similar NIR and IR bands to those reported for the known 17-electron $[\text{Ru}(\text{dppe})_2(\text{C}\equiv\text{CPh})\text{Cl}]^+$ radical cation. Remarkably, the dyad **3** has four stable redox states $+2/+1/0/-1$ where the second oxidation and first reduction processes take place at the porphyrin unit. Simulated absorption spectra on **1–4** at optimised geometries obtained by TD-DFT computations with the CAM-B3LYP functional are shown to be in very good agreement with the observed UV absorption spectra of **1–4**. The spectra of **1–4** and their oxidised and reduced species were interpreted with the aid of the TD-DFT data. Fluorescence measurements reveal that the dyads **3** and **4** are only weakly emitting compared to **1** and **2**, indicative of quenching of the porphyrinic singlet excited state by the ruthenium centre.

Received 26th January 2015,
Accepted 16th April 2015

DOI: 10.1039/c5dt00348b
www.rsc.org/dalton

Introduction

The combination of electron-rich group 8 metal complex(es) around a porphyrin core within the same molecular assembly can lead to new organometallic chromophores with remarkable optical properties.^{1,2} Furthermore, when the peripheral metallic fragments are redox-active, the redox-activity of these assemblies might be exploited for switching their linear optical (LO) and nonlinear optical (NLO) properties by means of electron-transfer.^{3,4} For instance, we showed that

tetra(ruthenium-chloride-ethynylphenyl)zinc(II) porphyrin (**ZnTRuEP**) presents particular cubic NLO properties which result from the association of the porphyrinic and Ru-based fragments (Chart 1).^{5–7} Akita and co-workers recently demonstrated that the fluorescence of a porphyrin linked to a $\text{CpM}(\text{P}^{\wedge}\text{P})$ unit *via* an acetylide, such as **A** and **B**, could be redox-switched.⁸ The neutral derivatives are essentially non-fluorescent due to an intramolecular redox quenching of the porphyrin excited singlet state by the organometallic substituent, while oxidation of the metal-alkynyl unit partially restores the red fluorescence characteristic of the Zn(II) porphyrin core. So far, only a handful of such organometallic conjugates have been reported^{8,9} despite their potential for use in molecular-based electronics or photonics.

While redox control of LO and NLO properties at the molecular level has ample precedence in the literature¹⁰ with metal acetylide derivatives,^{4,11} redox-control of the fluorescence with metal acetylide derivatives is much more rare in comparison.¹² However, no fluorescence yields were quoted for the fluorescent (“on”) states in these examples apart from the dyads **A** and **B** where low quantum yields of $\leq 1.5\%$ were measured.⁸ Although these examples clearly establish the proof of

^aInstitut des Sciences Chimiques de Rennes, ISCR-UMR CNRS 6226, Université de Rennes 1, 35042 Rennes Cedex, France. E-mail: christine.paul@univ-rennes1.fr, christine.paul@insa-rennes.fr

^bInstitut National des Sciences Appliquées, INSA-ISCR, 35043 Rennes Cedex; Université Européenne de Bretagne, France

^cDepartment of Chemistry, Durham University, Durham, DH1 3LE, UK. E-mail: m.a.fox@durham.ac.uk

† In memory of Ken Wade – a superb chemist and a true gentleman.

‡ Electronic supplementary information (ESI) available: NMR spectra for **1–4**, emission spectra for **3** and **4** at 77 K, additional CV plots for **3**, additional SEC spectra for **1–4**, molecular orbital data and Cartesian coordinates for optimised geometries of **1–4**. See DOI: 10.1039/c5dt00348b



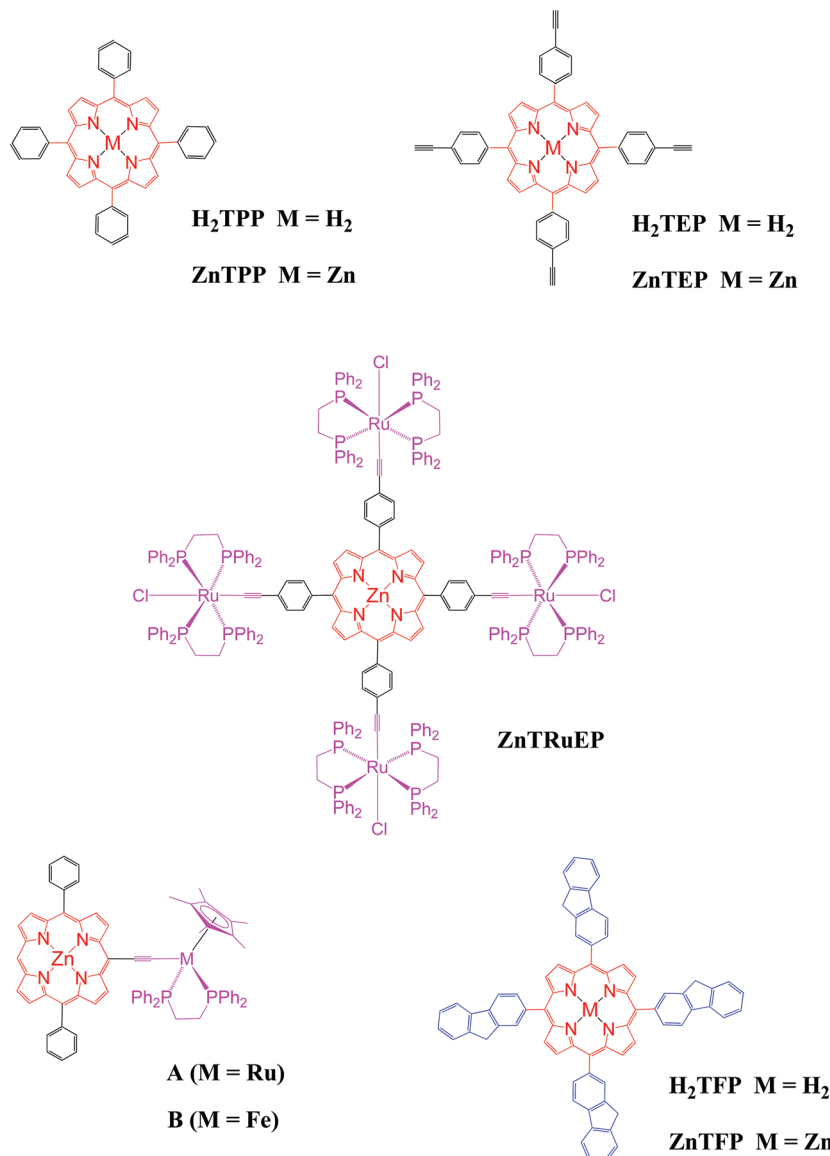


Chart 1 Previously reported porphyrins relevant to the current study.

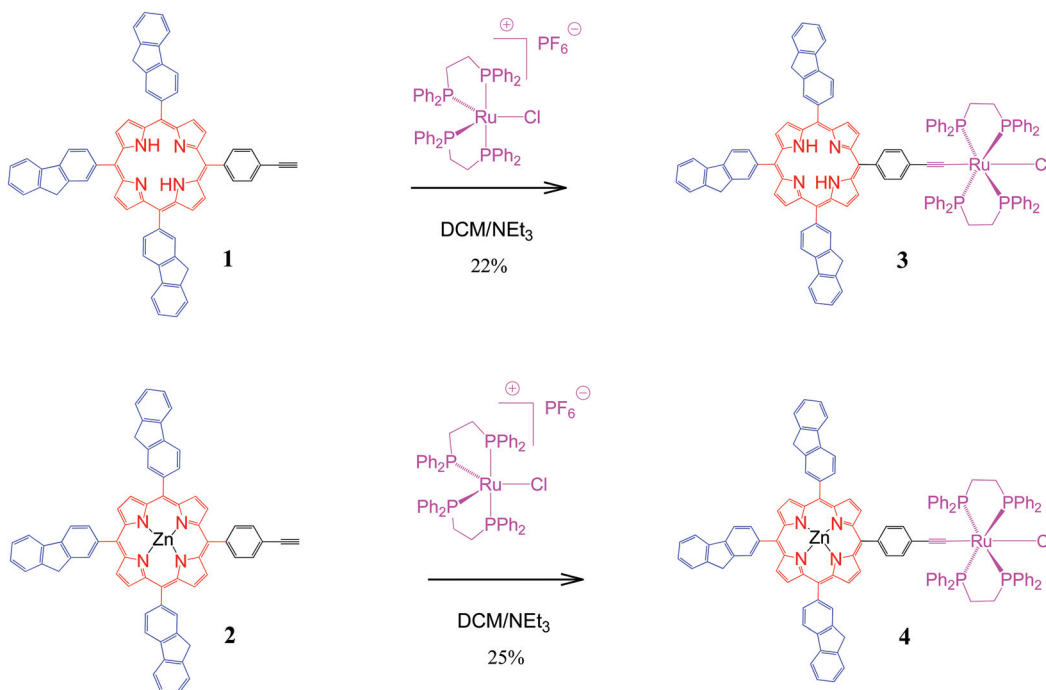
principle of fluorescence redox-switching for acetylide derivatives, more intense fluorescence in the “on” state is certainly desirable for any practical use compared to other systems developed so far.¹³

The low fluorescence yield reported in the case of **A**⁺ or **B**⁺ (“on” states) is not so surprising, given that the fluorescence of the **ZnTPP** core is intrinsically quite weak. In this respect, we reported the synthesis of zinc porphyrins possessing several fluorenyl arms (e.g. **ZnTFP**) and showed that the fluorescence of these derivatives was more intense than the corresponding phenyl (as opposed to fluorenyl) analogues (e.g. **ZnTPP**)^{14–16} eventually allowing their use as luminophores in OLEDs.⁵ In particular, a high fluorescence quantum yield ($\Phi_F = 24\%$) was evidenced for the metal-free tetrafluorenylporphyrin macrocycle (**H₂TFP**), demonstrating the good capacity of the fluore-

nyl units to enhance quantum yields by increasing the radiative deactivation process. Identifying new *meso*-tetraarylporphyrin conjugates resembling **ZnTRuEP**, **A** or **B** – but featuring fluorenyl groups instead of phenyl ones on the porphyrin core – may thus be an attractive approach to isolate new redox-switchable conjugates that would have more desirable fluorescence properties in the “on” (oxidised) state.

This work describes a first contribution toward this aim using the well-established¹⁷ Ru(dppe)₂Cl metal-acetylide fragment as electrophore for redox-controlling the fluorescence of porphyrins with pendant fluorenyl arms. Thus, the syntheses and characterisation of the new dyads **3** and **4** from the recently synthesised^{18,19} ethynylphenyltrifluorenylporphyrins **1** and **2** respectively (Scheme 1) and the luminescence properties of these compounds are reported. The spectral properties of





Scheme 1 Syntheses of new dyads 3 and 4.

the four porphyrins **1–4** and their various oxidised and reduced species are also examined in detail by UV spectroelectrochemistry (SEC) and, for **3** and **4**, by IR and NIR spectroelectrochemistry. These experimental studies are complemented by DFT computations to understand the nature of the observed absorption bands. The use of the new acetylidyne complexes **3** and **4** for redox-switching of their optical properties is briefly discussed.

Results and discussion

Syntheses and characterisation

The new dyad **3** was formed from the reaction of the ethynyl-phenyltrifluorenylporphyrin **1** with the 16-electron five-coordinate ruthenium complex $[\text{RuCl}(\text{dppe})_2]\text{PF}_6$ in dichloromethane (DCM) followed by triethylamine (NEt₃) (Scheme 1).²⁰ The latter was used in excess to avoid an inseparable mixture of the starting material **1** and the desired product **3**. The reaction was considered complete when the singlet peak of the terminal alkyne at 3.3 ppm disappeared on monitoring the mixture by ¹H NMR spectroscopy prior to work-up, which gave a greenish-brown solid identified as **3**. Dyad **4** was made from **2** using a similar procedure.

The dyads **3** and **4** were characterised by multinuclear NMR spectroscopy, mass spectrometry and elemental analyses. ³¹P NMR spectra for **3** and **4** showed singlets at 49.7 and 50.0 ppm respectively, corresponding to four equivalent phosphorus atoms in the dppe ligands coordinated to the ruthenium group. The peaks in the ¹H NMR spectrum of **4** can be identified by direct comparison with the ¹H NMR spectra of **2** and a

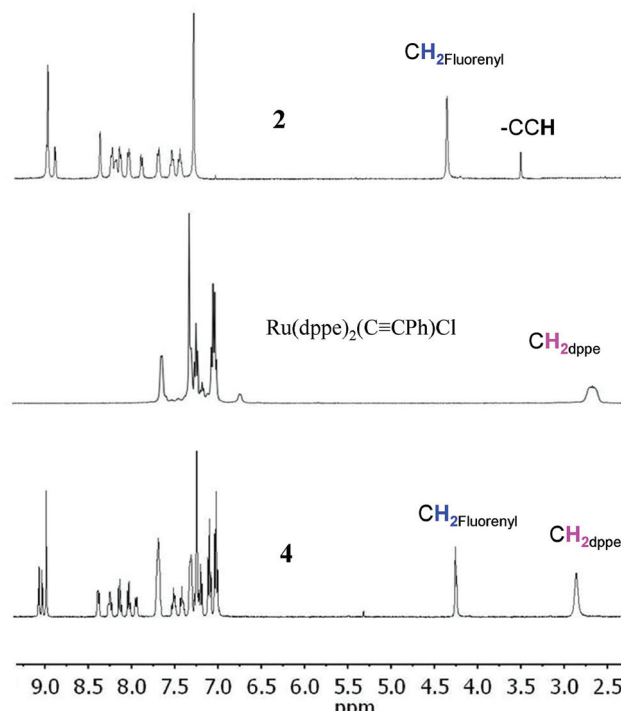


Fig. 1 ¹H NMR spectra (400 MHz, in CDCl₃) of zinc porphyrin **2**, Ru(dppe)₂(C≡CPh)Cl and the new dyad **4**.

model compound²¹ RuCl(C≡CPh)(dppe)₂ (Fig. 1). The spectrum of **4** contains a broad multiplet at 2.8 ppm corresponding to the eight CH₂ dppe protons. Two peaks, a singlet at





4.20 ppm (2H), and another at 4.22 ppm (4H), characterise the CH_2 protons of the fluorenyl units. The peaks between 7.0 and 7.4 ppm and the overlapped peak at 7.8 ppm are from the phenyl groups of the dppe ligands. Between 7.4 and 8.5 ppm, the seven peaks that correspond to the fluorene groups are identified along with two doublets at 7.04 and 7.98 ppm corresponding to the phenylene unit at the porphyrin (Fig. S1‡). In addition, the β pyrrolic protons are identified by the peaks at around 9 ppm. The ^1H NMR spectrum of **3** differs from that of **4**, with a singlet at -2.6 ppm characterizing the porphyrin NH protons. The ^{13}C NMR spectra for **1–4** also show the expected peaks although many are overlapped – there are 43 unique carbons in **1** and **2** and 52 in **3** and **4** (Fig. S2‡).

Absorption and emission spectroscopy

The UV-visible absorption spectra were recorded at room temperature for **1–4** (Fig. 2 and Table 1). In all cases, the spectra exhibit an intense B-(Soret) band with a maximum absorption around 425 nm and several lower-energy Q-bands. Four charac-

teristic Q-bands are observed for the free-base porphyrins **1** and **3** (two of them overlapped in **3**), while only two bands are observed for the Zn(II) complexes **2** and **4**, as is usual in metalloporphyrins. A characteristic blue shift is observed for all these bands upon metallation with zinc. In addition, a broad band centred around 275 nm is seen for **1–4**, which corresponds to the absorption of the three fluorenyl arms of the porphyrin.

The emission spectra of these compounds were recorded upon excitation of the Soret band (Fig. 3). Depending on their nature (free base or metallated porphyrin) they consist of several sub-bands assigned to a vibronic progression from the Q-state: for **3**, the band near 720 nm assigned as Q(2,0) is very weak and appears often as an extended tail on the Q(1,0) band. The main fluorescence bands are blue-shifted upon metallation. For **3**, the strongest emission band Q(0,0) is typically around 600 nm and the second peak, *i.e.* Q(1,0), appears at \sim 650 nm. Compounds **1** and **2** without any Ru acetylide substituents have more intense fluorescence in solution than **3** and **4**. Porphyrin **1** has a luminescence quantum yield of 21% which is higher than that of the reference H_2TPP (12%) and comparable to that of H_2TFP (24%). The Zn(II) porphyrin **2** has a quantum yield of 7%, again higher than that of the TPP analogue ZnTPP (3.3%). After substitution of **1** with the Ru complex to generate the dyad **3**, the fluorescence quantum yield drops to 1.5%, comparable to the values reported for **A⁺** and **B⁺**. Dyad **4** with the Zn(II) porphyrin is much more weakly emissive ($\Phi = 0.02\%$), similar to that determined for ZnTRuEP , **A** and **B**. It seems that the complexation of the porphyrin ligand by Zn(II) facilitates the non-radiative deactivation processes. The quenching of the porphyrin emission by the ruthenium unit is apparently less efficient for the free base porphyrins than for the zinc porphyrins. The emission spectra of **3** and **4** at 77 K are shown in Fig. S3.‡

Electrochemistry

Cyclic voltammetry (CV) data of tetraarylporphyrins generally show two oxidation and two reduction waves corresponding to oxidation and reduction at the porphyrin unit. These waves are present in the CV measurements carried out here for **1** and **2** where the first oxidation and reduction waves are reversible (Fig. 4 and Table 2). Table 2 also lists reported CV values for related porphyrins (Chart 1) where zinc porphyrins are easier to oxidise by \sim 0.1 V and more difficult to reduce by \sim 0.2 V compared to the metal-free porphyrin analogues. The compounds **1** and **2** at 2.18 V and 2.26 V respectively have the smallest oxidation-reduction potential differences of the porphyrins listed in Table 2. Irreversible oxidation waves at even more positive potentials are also found in the porphyrins listed, which correspond to oxidations at the fluorenyl groups in **1** and **2**.

The CV data for the ruthenium–porphyrin complexes, **3** and **4**, reveal reversible oxidation waves at -0.02 and 0.01 V respectively due to oxidations at the ruthenium ethynyl units at similar potentials to the ferrocenium/ferrocene couple.^{29,30} For comparison, $\text{Ru}(\text{dppe})_2(\text{C}\equiv\text{CPh})\text{Cl}$ has an oxidation potential

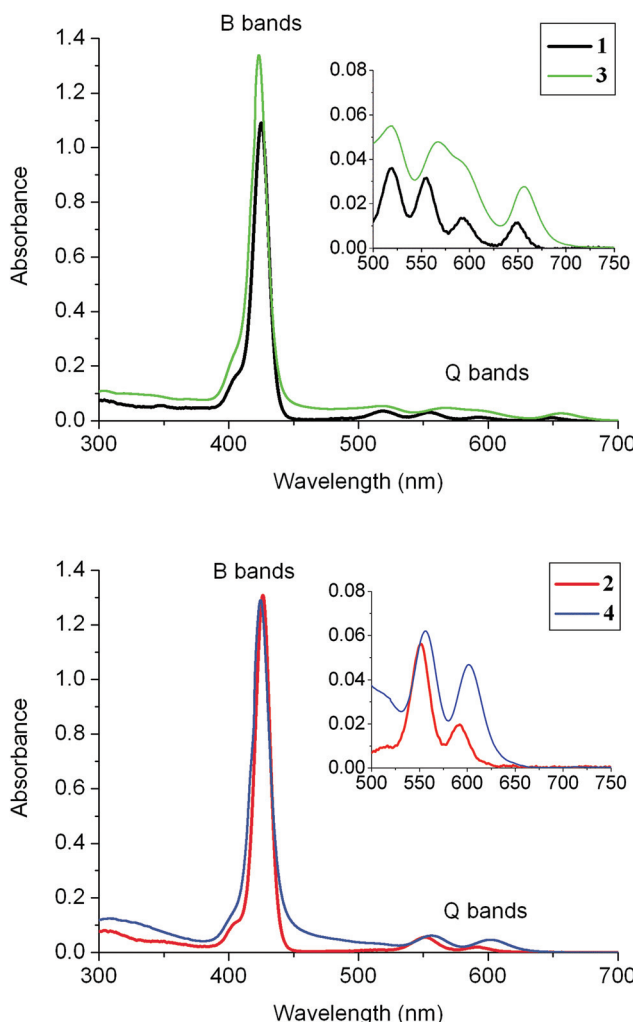


Fig. 2 Absorption spectra (in DCM) of the new dyads **3** and **4** (10^{-5} M) at room temperature. The corresponding precursors **1** and **2** are included for comparison.

Table 1 Photophysical data for porphyrins **1–4** and related compounds in DCM at 298 K

	$\lambda_{\text{max}}^a/\text{nm}$	$\lambda_{\text{max}}^b/\text{nm}$	$\lambda_{\text{max}}/\text{nm}$	$\lambda_{\text{em}}/\text{nm}$	$\Phi_f^c\ %$	Ref.
	UV band	Soret band	Q bands			
1	275	425	518, 555, 594, 649	657, 700	21	This work
2	273	426	554, 595	607, 655	7	This work
3	263	423	520, 568, 590, 657	659, 718	1.54	This work
4	264	425	557, 602	606, 651	0.02	This work
H₂TPP	—	417	513, 548, 589, 646	650, 714	12	22
H₂TFP	272	426	519, 557, 593, 649	661, 725	24	23
ZnTFP	264	428	555, 601	608, 657	8.5	24
ZnTEP	302	424	552, 594	—	—	6
ZnTPP	—	421	556, 603	603, 650	3.3	This work
ZnTRuEP	327	418	452, 563, 615	601, 652	0.02	This work

^a Wavelengths of the absorption maxima in the UV region (200–400 nm range). ^b Wavelengths of the absorption maxima in the Soret or B band region (400–450 nm range). ^c Fluorescence quantum yields using **H₂TPP** in toluene as standard ($\Phi_f = 0.12$)²² following excitation into the Soret bands.

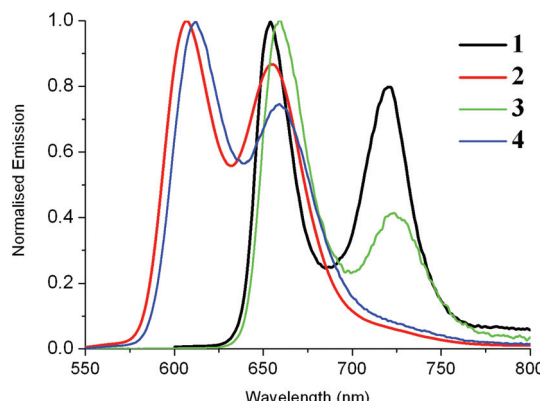


Fig. 3 Emission spectra (in DCM) of the new dyads **3** (10^{-5} M) and **4** (10^{-6} M) at room temperature and comparison with emissions of **1** and **2**.

of 0.01 V²⁷ which shows that the porphyrin moieties have very small effects on the potentials corresponding to the ruthenium ethynyl moieties, as found for **ZnTRuEP**.⁷ The presence of the ruthenium redox centres results in the oxidation waves associated with the porphyrin units being shifted to more positive potentials by ~ 0.06 V in **3** and **4**. This trend follows for the reduction wave potential of **4** but does not follow for **3** where its reduction wave potential is more negative by 0.05 V. Unlike their porphyrin precursors **1** and **2**, the second oxidation and reduction waves at the porphyrin units in **3** and **4** are irreversible. There is an irreversible oxidation wave at 0.89 V²⁷ for Ru (dppe)₂(C≡CPh)Cl which suggests that such irreversible waves are expected in **3** and **4** in the same potential range as the second oxidation waves at the porphyrin units. The observed two irreversible oxidation waves for **3** and **4** (Table 2 and Fig. S4[‡]) support this.

Spectroelectrochemistry

Spectroelectrochemistry (SEC) measurements were carried out on the four porphyrins **1–4**, to obtain the absorption spectra and establish the stabilities of their oxidised and reduced species. Absorption measurements of the oxidised and reduced species for all porphyrins are listed in Table 3. Apart from our published study,⁷ there is only one study on the parent porphyrins using a thin-layer SEC cell and two spectroscopic studies on porphyrin radical anions generated electrochemically. The reported data from these studies are shown in Table 3 for comparison.

UV-Visible spectroelectrochemistry. The first oxidation and first reduction processes for **1** were shown to be reversible in the SEC cell (Fig. 5 and Table 3). The absorption spectrum corresponding to the cation of **1** showed a significant change from the neutral species where the original Soret band at 424 nm is replaced by strong bands at 464 and 690 nm. The spectrum of the cation is similar to that reported for the cation of **H₂TPP** by SEC. The spectrum of the anion by reduction of **1** has the Soret band diminished in intensity and the Q-bands still evident with addition of more, weak, low-

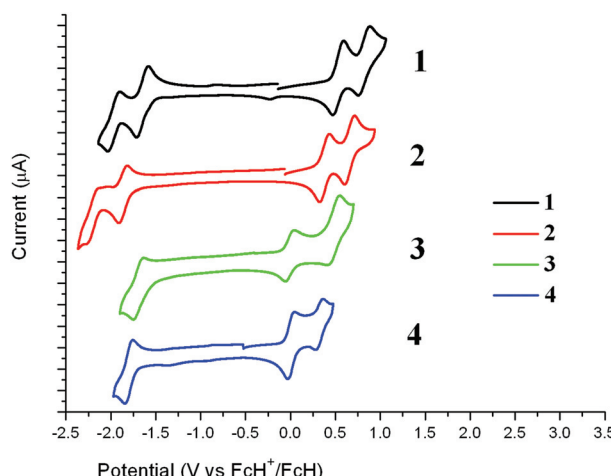


Fig. 4 Cyclic voltammograms for **1–4** in DCM in the presence of 0.1 M [Bu₄N][PF₆] as the supporting electrolyte. The current is scaled at 5 μA between each tick mark.



Table 2 Electrochemical data for porphyrins **1–4** and related compounds

	E_{ox}^1	E_{ox}^2 ^a	E_{ox}^3 ^a	E_{red}^1	E_{red}^2 ^b	$E_{\text{ox}}^1 - E_{\text{red}}^1$	Ref.
1	0.53	0.82	<i>1.43</i>	−1.65	−1.98	2.18	This work
2	0.39	0.66	<i>1.35</i>	−1.87	−2.27	2.26	This work
3	−0.02 ^c	0.48	<i>0.81, 0.94</i>	−1.70	−2.15	1.68	This work
4	0.01 ^c	0.32	<i>0.50, 0.63</i>	−1.80	−2.19	1.81	This work
H₂TPP	0.53	0.87	<i>1.95</i>	−1.78	−2.12	2.31	25
ZnTPP	0.46	0.72	—	−1.90	−2.28	2.36	25
H₂TFP	0.58	0.90	<i>1.50</i>	−1.78	−2.12	2.36	26
ZnTFP	0.41	0.71	<i>1.40</i>	—	—	—	26
Ru(dppe)₂(C≡CPh)Cl	0.01 ^c	0.89	—	—	—	—	27
H₂TEP	0.58	0.90	<i>1.05, 1.36</i>	−1.62	−1.95	2.20	28
ZnTEP	0.46	0.72	—	−1.90	−2.32	2.36	28
ZnTRuEP	0.03 ^c	0.41	0.70	—	—	—	6

^a Values in italics are anodic potentials of irreversible waves. ^b Values in italics are cathodic potentials of irreversible waves. ^c Oxidation at the ruthenium unit.

Table 3 Absorption data for **1**, **2**, **3** and **4** and their oxidised and reduced species obtained by spectroelectrochemistry (SEC) in 0.1 M [Bu₄N][PF₆]/DCM at 298 K

Porphyrin	<i>n</i>	$\lambda_{\text{max}}/\text{nm}$	$\lambda_{\text{max}}/\text{nm}$	$\lambda_{\text{max}}/\text{nm}$	$\lambda_{\text{max}}/\text{nm}$
		UV band	“Soret bands”	“Q bands”	NIR band
[1]ⁿ	0	262 (65), 304 (39)	424 (527)	519 (27), 556 (20), 596 (8), 649 (9)	
	+1	261 (58), 322 (36)	464 (341)	632 (sh, 15), 690 (76)	
	“+2”	384 (70)	440 (sh, 106), 485 (126)	670 (158)	
	−1	257 (59), 305 (45)	425 (238), 457 (sh, 43)	519 (20), 557 (16), 601 (12), 656 (13), 704 (5)	791 (5), 878 (6), 942 (sh, 4)
[2]ⁿ	0		427 (479)	554 (22), 614 (14)	
	“+1”		425 (140), 460 (94)	689 (22)	874 (12)
[3]ⁿ	“−1”	318 (70)	437 (224)	570 (40), 614 (46), 722 (8)	835 (15)
	0	261 (133)	423 (478)	520 (20), 559 (18), 594 (9), 650 (7)	840 (4), 1234 (3)
	+1	262 (117)	424 (404)	705 (57)	
[4]ⁿ	+2		460 (195)	517 (sh, 20), 561 (18), 606 (17), 657 (9), 722 (8)	839 (sh, 3)
	−1	260 (153)	411 (94), 466 (sh, 40)	553 (27), 597 (15)	
	0		424 (480)	553 (26), 593 (13)	817 (5), 1302 (2)
[H₂TPP]ⁿ	+1		426 (435)	551 (20), 693 (19)	880 (7)
	“+2”		425 (238), 454 (75)	572 (32), 616 (34)	793 (7)
	“−1”	261 (153), 312 (77)	437 (473)	513 (18), 548 (8), 590 (5), 647 (4)	
[ZnTPP]ⁿ	0 ^a		418 (466)	660 (49)	
	+1 ^b		417 (sh, 245), 436 (368)	625 (9), 683 (13), 705 (sh, 12)	765 (9), 873 (9)
	−1 ^a		405 (85), 430 (sh, 80), 448 (89)	548 (20), 595 (23)	
[ZnTFP]ⁿ	−2 ^a		415 (sh, 61), 438 (82)	545 (21), 585 (3)	
	0 ^c		419 (560)	515 (10), 560 (10), 610 (12)	
	+1 ^c	365 (35)	409 (190), 460 (33)		770 (10), 840 (3)

^a Bulk electrolysis, [Et₄N][ClO₄], DMF, ref. 31. ^b Ref. 32. ^c Bulk electrolysis, [Pr₄N][ClO₄], THF, ref. 33.

energy bands between 450 and 950 nm. Such weak, broad low-energy bands are also observed for the anion of **H₂TPP** by bulk electrolysis.

A second SEC experiment was carried out on **1** in order to obtain the spectrum of the dication by two-electron oxidation. The two intense monocation bands at 464 and 690 nm were changed to two bands with smaller intensities at 440 and 485 nm and a broad, more intense band at 670 nm (Fig. S5†). However, on back reduction the monocation spectrum was subtly different, displaying bands at 460 and 680 nm. This suggests that the dication is not stable under these thin-layer SEC cell conditions and the spectral data listed in Table 2 are thus labelled “2+”. Given the obvious similarities between the

initial neutral species and the neutral species on back reduction, it is assumed here that the spectrum of pure dication would resemble “2+”.

SEC studies on **2** were less satisfactory. A spectrum of an oxidised species was obtained but on back-reduction the spectrum of neutral **2** was not fully restored. There were weak bands present at 520 and 650 nm on back reduction which imply that the Zn ion was replaced by protons during the process. A similar spectrum was found from back-oxidation on a second experiment investigating the reduction process of **2**. The loss of the Zn ion in both processes suggests that zinc porphyrins with fluorenyl groups are susceptible to metal loss on oxidation and reduction processes. The spectra for the



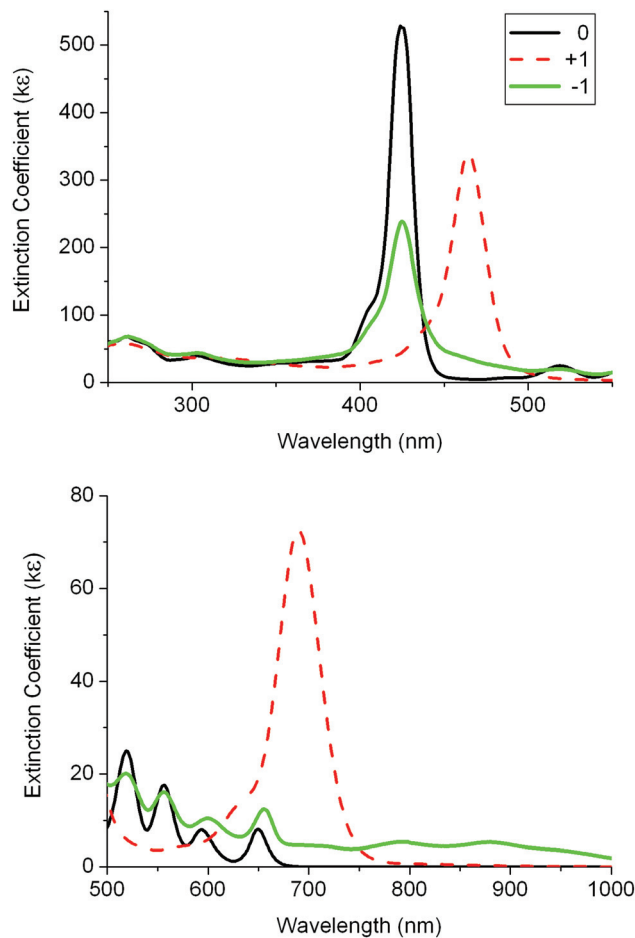


Fig. 5 UV-visible absorption spectra for **1** and its oxidised and reduced species in 0.1 M $[\text{Bu}_4\text{N}][\text{PF}_6]$ /DCM using a thin-layer spectroelectrochemistry (SEC) cell.

oxidised and reduced species “+1” and “−1” of **2** are listed in Table 3 and shown in Fig. S6.‡ While they are not robust species, some bands probably are from the expected monocation and monoanion of **2**. The similarity of the “+1” bands to the reported data of the monocation species of ZnTPP supports this assumption.

Spectra were recorded for two oxidation species and a reduction species of **3** (Fig. 6 and Table 3). The original spectrum for the neutral species of **3** was recovered after recording these oxidised and reduced species. The first oxidation process showed little changes to the Soret and Q bands suggesting that the porphyrin unit is not involved in the oxidation process.⁷ The second oxidation process showed the same dramatic changes involving the Soret and Q bands as found for the first oxidation of **1** (Table 3 and Fig. S7‡). The spectrum on reduction of **3** has the Soret band intensity diminished and many weak bands between 450 and 850 nm. This resembles the spectrum for the reduced species of **1** and indicates that the porphyrin unit is reduced.

As in **3**, the first oxidation process of **4** showed little change to the Soret and Q-bands (Table 3 and Fig. S8‡). On further

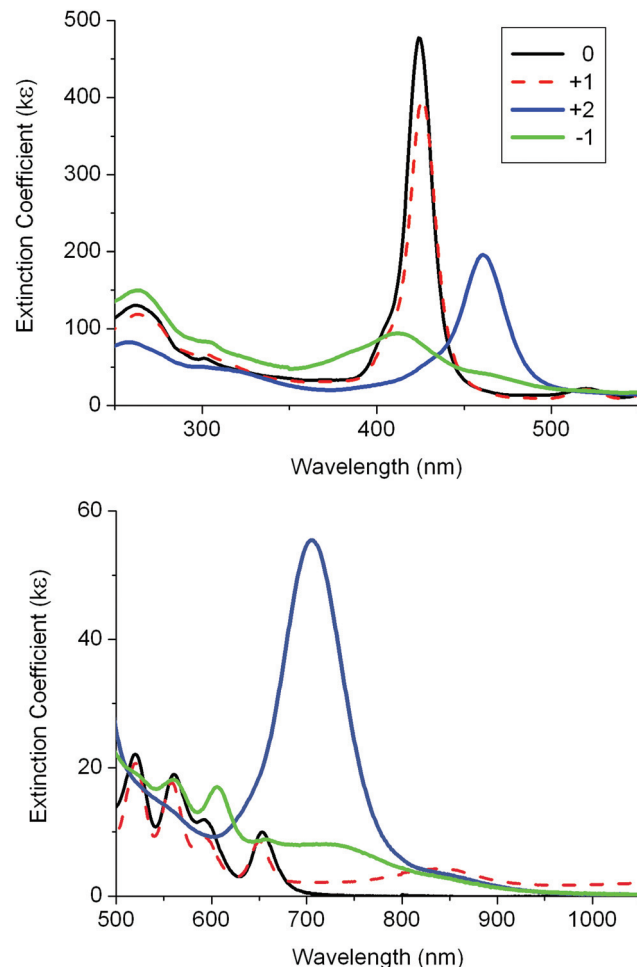


Fig. 6 UV-visible absorption spectra for **3** and its oxidised and reduced species in 0.1 M $[\text{Bu}_4\text{N}][\text{PF}_6]$ /DCM using a SEC cell.

oxidation, there are notable changes to the Q bands with new, weak, low-energy bands at 693 and 880 nm. However, back-reduction did not revert to the original spectrum corresponding to **4** as minor peaks at 520 and 650 nm were present. In fact, the back-reduction spectrum appears as a mixture of neutral **3** and **4**. The loss of the zinc(II) metal presumably takes place during the second oxidation process. Reduction of **4** also resulted in some loss of the zinc on back oxidation. It is a very important detrimental process and one which needs to be overcome if fatigue-resistant redox-switchable systems are to be developed with such molecules. The spectra recorded for “+2” and “−1” are assumed to represent the spectra of the dication and monoanion of **4**. There are obvious similarities between these spectra and the “+1” and “−1” spectra of the zinc precursor **2**. More importantly, these spectra are different from those of the corresponding species of **1** and **3**.

NIR and IR spectroelectrochemistry. Both near-IR (NIR) spectra for the first oxidised species of the ruthenium complexes, **3** and **4**, contain two weak bands at around 12 000 and 8000 cm^{-1} (Fig. 7 and Table 4). These bands are characteristic of the arylethynylruthenium moiety on oxidation. For example,

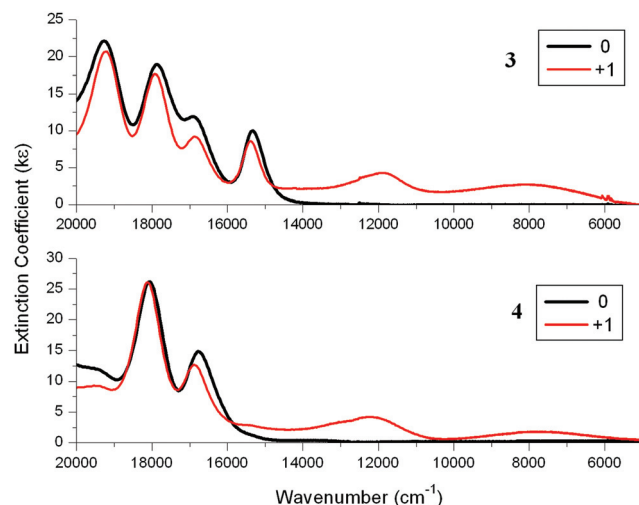


Fig. 7 Near-IR (NIR) absorption spectra for **3** (top) and **4** (bottom) and their cations in 0.1 M $[\text{Bu}_4\text{N}][\text{PF}_6]$ /DCM using a SEC cell.

the spectrum of the monocation of $\text{Ru}(\text{dppe})_2(\text{C}\equiv\text{CPh})\text{Cl}$ shows two weak NIR bands at around 12 000 and 9000 cm^{-1} (Fig. S9‡).^{29,30,34} Unlike the precursors **1** and **2** which contain very weak $\text{C}\equiv\text{C}$ bands, the arylethynylruthenium complexes **3** and **4** contain strong $\text{C}\equiv\text{C}$ bands at 2068 cm^{-1} and so IR spectroelectrochemistry experiments were also carried out on these ruthenium complexes. On oxidation, the $\text{C}\equiv\text{C}$ bands corresponding to the neutral species disappeared and $\text{C}\equiv\text{C}$ bands at 1910 cm^{-1} appeared along with the tails of the NIR bands (Fig. S10 and S11‡). The energy differences of 158 cm^{-1} for these $\text{C}\equiv\text{C}$ bands on oxidation are typical of arylethynylruthenium complexes, with 165 cm^{-1} having been reported for $\text{Ru}(\text{dppe})_2(\text{C}\equiv\text{CPh})\text{Cl}$.^{30,34} These NIR and IR data for the cations of **3** and **4** indicate that the porphyrin units have little influence on the spectral properties associated with the Ru units and may be considered as spectators.

Computations

Geometry optimisations on **1–4** were carried out with the hybrid-DFT functional method (B3LYP) in order to aid interpretation of their observed spectroscopic data, with **1'–4'** denoted for DFT-optimised geometries to distinguish from the

physical geometries. Metal-free porphyrins are difficult to model correctly for comparison between observed and calculated spectroscopic data as the two hydrogens at the nitrogens of the porphyrin unit are fluctual in solution. The most stable conformer **1'** involves the two hydrogens at opposite nitrogen atoms in the porphyrin centre. Three conformers of **1**, where two hydrogens are at adjacent nitrogens, were also optimised and are 7.0, 7.1 and 7.2 kcal mol^{-1} less stable in energy than **1'**. The predicted electronic structures and spectroscopic data from these three conformers are somewhat similar to that of **1'** so only the geometries of **1'** and, by implication, **3'** with hydrogens at opposite nitrogens are looked at in detail here.

Electronic structure calculations reveal the expected frontier orbitals (HOMO and LUMO) located at the porphyrin units for **1'** and **2'** (Fig. 8). In **1'**, the LUMO+1 and HOMO–1 orbitals are also at the porphyrin unit (Gouterman four-electron four-orbital model).³⁵ While the LUMO and LUMO+1 orbitals are degenerate, the HOMO–1 is 0.4 eV lower in energy compared to HOMO (Table S1‡). The orbital make-up in **2'** is different due to an occupied orbital involving zinc so the 'four orbitals' in **1'** become five in **2'** (Table S2‡). This would explain the different Q-band characteristics in observed absorption spectra for metal-free and zinc porphyrins. Comparison of the HOMO and LUMO energies for **1'** and **2'** with the first oxidation reduction half-wave potentials in Table 1 shows the logical trends in the LUMO energies and the HOMO–LUMO energy differences. However the higher predicted HOMO energy in **1'** by 0.1 eV compared to **2'** does not support the fact that **2** is easier to oxidise by 0.14 V compared to **1**. Calculated HOMO energies for metal-free porphyrins have been reported to be higher than for zinc porphyrins³⁶ and it is assumed here that the zinc contribution to the stability of the HOMO energies is over-estimated in the computations.

For the ruthenium dyad **3'**, the HOMO, HOMO–1 and HOMO–2 with similar energies of –4.61, –4.81 and –4.91 eV are mainly at the ethynylruthenium unit whereas the degenerate LUMO and LUMO+1 are on the porphyrin unit (Fig. 9 and Table S3‡). While the LUMO is essentially located on the porphyrin only, the porphyrin contributes significantly (29%) to the HOMO which is quite surprising when the porphyrin group has little influence on the observed oxidation potential of **3** (–0.02 V) compared to 0.01 V for $\text{Ru}(\text{dppe})_2(\text{C}\equiv\text{CPh})\text{Cl}$.

Table 4 NIR and IR absorption data for **3**, **4**, $\text{Ru}(\text{dppe})_2(\text{C}\equiv\text{CPh})\text{Cl}$, **ZnTRuEP** and their monocations obtained by spectroelectrochemistry (SEC) in 0.1 M $[\text{Bu}_4\text{N}][\text{PF}_6]$ /DCM at 298 K

Compound	<i>n</i>	λ/cm^{-1} NIR band	$\nu(\text{C}\equiv\text{C})/\text{cm}^{-1}$	Reference
[3]ⁿ	0		2068	
	+1	11 880 (4), 8100 (3)	1910	This work
[4]ⁿ	0		2068	
	+1	12 210 (5), 7680 (2)	1910	This work
$[\text{Ru}(\text{dppe})_2(\text{C}\equiv\text{CPh})\text{Cl}]^n$	0		2075	
	+1	12 040 (10), 9080 (1)	1910	34
[ZnTRuEP]ⁿ	“+4”	12200, 8350		7



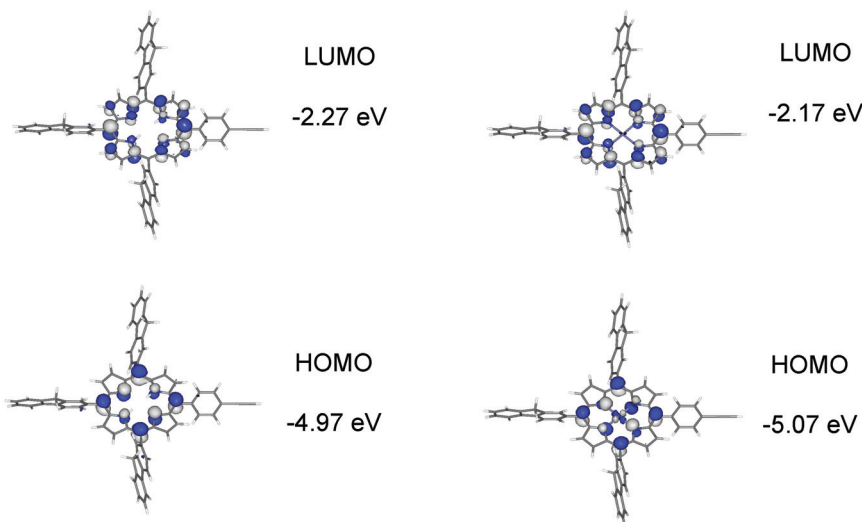


Fig. 8 Frontier molecular orbitals for **1'** and **2'** plotted with a contour value of ± 0.04 ($e \text{ bohr}^{-3}\right)^{1/2}$.

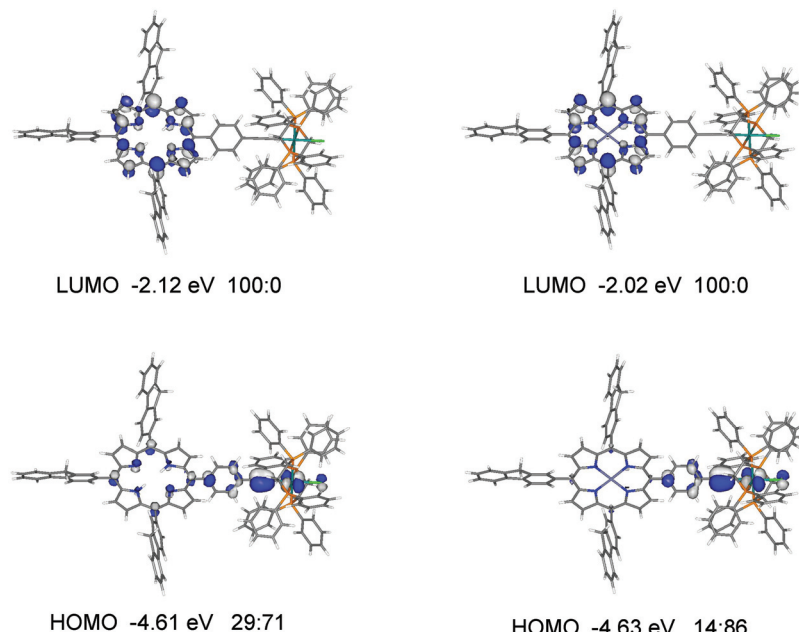


Fig. 9 Frontier molecular orbitals for **3'** and **4'**. The ratios listed correspond to % orbital contributions on the porphyrin and $[(C_6H_4C\equiv C)Ru(dppe)_2Cl]$ fragments.

A similar orbital make up to **3'** is found for **4'** (Fig. 9 and Table S4†) with one notable difference: the orbital with ruthenium character (HOMO-2) in **3'** is not present in the occupied orbitals of similar energies for **4'**, presumably due to the contributions of the zinc atom to the orbitals in **4'**. The HOMO in **4'** has considerably less porphyrin contribution (14%) than the HOMO in **3'** (29%) yet their energies are very similar at -4.63 and -4.61 eV respectively. The trend of the HOMO energies is in good agreement with the observed oxidation potentials (Table 2).

TD-DFT computations were carried out on all geometries **1'-4'** to simulate the absorption spectra and to aid assignments of the bands in the observed spectra of **1-4** and, by inference, assign the bands of the oxidised and reduced species. The CAM-B3LYP functional is used here instead of B3LYP as it is necessary to correctly model charge transfer over long distances³⁷ for dyads like **3** and **4**. One disadvantage with the predicted TD-DFT data is that the vibronic couplings typically observed in the Q-bands for porphyrins are not taken into account. While open-shell optimisations of these oxidised and



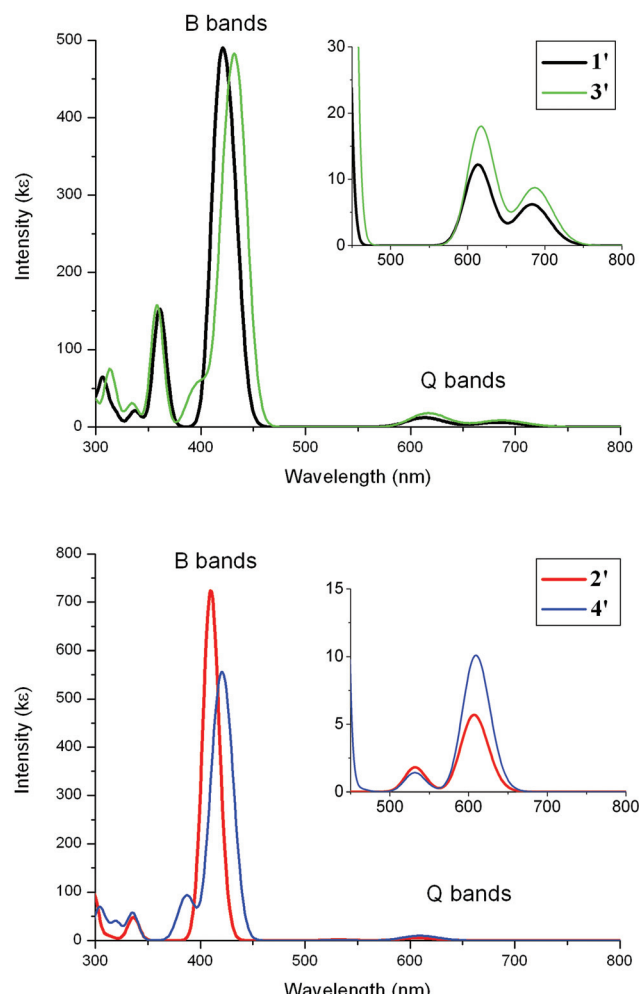


Fig. 10 TD-DFT absorption spectra for **1'-4'**. The bands were simulated using a half-height width of 0.08 eV.

reduced species can be carried out here, predicted open-shell TD-DFT data on porphyrin geometries are generally unreliable as shown elsewhere.³⁸

Simulated absorption spectra on **1'-4'** from TD-DFT data are shown in Fig. 11. The observed strong Soret(B-) and the relatively weaker Q-bands are reproduced well computationally in **1'** and **2'** assuming that the computed Q-bands would be split by vibronic couplings. The predicted Soret bands at 410–431 nm are in good agreement with the observed maxima of 423–428 nm (Table 5). The computed lowest energy Q-bands are also in accord with observed lowest energy Q-bands as shown in Table 5. Computed extinction coefficients for these bands also reproduce similar values to those observed.

The Soret or B-bands arise from allowed HOMO–1 → LUMO/LUMO+1 transitions where the π and π^* orbitals largely overlap in the porphyrin unit in **1'** and **2'** (Fig. 11). The weaker Q-bands in **1'** result from two HOMO → LUMO/LUMO+1 transitions where the HOMO has significant N p-orbital character. The weaker Q-bands in **2'** are from the four HOMO/

HOMO–2 → LUMO/LUMO+1 transitions where the HOMO and HOMO–2 have substantial zinc characters (Fig. 11).

In the case of the complexes **3'** and **4'**, the simulated Soret and Q-bands are in agreement with observed absorption spectra for **3** and **4** (compare Fig. 10 with Fig. 2). As the Q-bands for **3'** resemble **1'** and **4'** with **2'**, the orbital contributions from the arylethynylruthenium to these bands are very small (Fig. 10). Any bands resulting from transitions involving the ruthenium moiety and the porphyrin have low oscillator strengths – these are charge-transfers – relative to the local porphyrin-porphyrin transitions and thus have little impact on the overall spectral patterns for **3'** and **4'**.

Oxidation of **1** to $[1]^+$ would involve removal of an electron from the HOMO, forming a singly occupied molecular orbital SOMO, and thus result in significant changes in the energies of both HOMO (which would then become highest occupied single orbital, α -HOSO, and lowest unoccupied single orbital, β -LUSO, in open-shell computation data) and HOMO–1 (α -HOSO–1 and β -HOSO). Since the transitions corresponding to Soret bands and Q-bands involve HOMO and HOMO–1, dramatic changes in these bands are expected in the absorption spectra on oxidation of **1** to $[1]^+$. These changes are observed experimentally, with the bands at 464 and 690 nm assigned to π (porphyrin) → π^* (porphyrin) and π (porphyrin) → π^* (N-character porphyrin) transitions, similar to those responsible for the Soret and Q-bands of **1**. The 690 nm band lacks the vibronic couplings typically found in neutral porphyrins due to loss of orbital symmetries in the orbital make-up of the radical cation $[1]^+$.

Reduction of **1** to $[1]^-$ adds an electron to the LUMO but this picture is complicated with the LUMO and LUMO+1 being degenerate in **1**. When an electron is added, the LUMO becomes a SOMO (α -HOSO and β -LUSO). The observed spectrum of $[1]^-$ retains several bands observed in **1** which are the transitions involving the largely unchanged degenerate molecular orbital LUMO+1 *i.e.* responsible for the Soret and Q-bands. There are several unique bands in $[1]^-$ which arise from transitions involving the SOMO and all would involve porphyrin orbitals. Similar band assignments would apply to the spectra of the oxidised and reduced species of **2**. The Q-bands in **2** are quite different to those in **1** due to the zinc contribution but the overall spectral changes on oxidation and reduction of **2** follow those of **1**.

The first oxidations of **3** and **4** to $[3]^+$ and $[4]^+$ take place at the ethynylruthenium units where the HOMOs are located. As mentioned earlier, the charge transfer transitions involving the HOMO and HOMO–1 – which are essentially two ethynylruthenium d– π orbitals orthogonal to each other^{30,39} – give bands too weak to be observed above the strong Soret and the relatively weaker Q-bands from local porphyrin-porphyrin transitions in the absorption spectra of **3** and **4**.

Removal of an electron from the HOMO in **3** would lead to a SOMO (α -HOSO and β -LUSO) on the ethynylruthenium moiety and thus a low-energy transition from an ethynylruthenium orbital (HOMO–1 in **3**; α -HOSO–1 and β -HOSO in $[3]^+$) into another ethynylruthenium orbital (SOMO; α -HOSO and

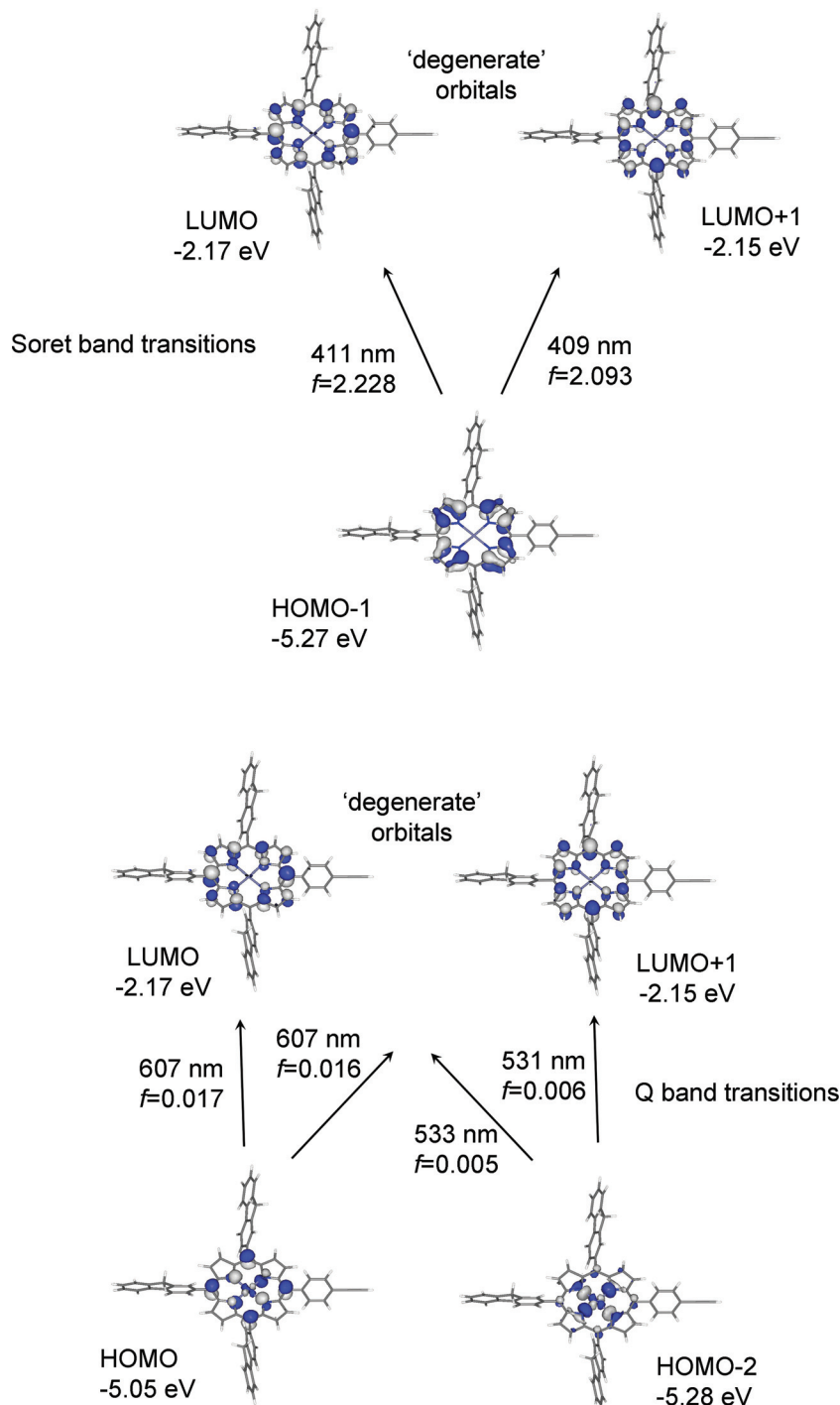


Fig. 11 Orbitals involved in the B-(Soret) and Q-bands for **2** based on TD-DFT data with computed wavelength and oscillator strength (f) listed for each transition.

β -LUSO) is expected. The weak NIR band of 8100 cm^{-1} observed for $[3]^+$ is assigned to this formally β -HOSO \rightarrow β -LUSO transition. A second weak NIR band of 11 880 cm^{-1} is also the result of a transition involving the ethynylruthenium SOMO since similar NIR transitions are found in related ethynylruthenium cations (Table 4). No obvious changes are found

for the Soret and Q-bands on oxidation of $[3]$ to $[3]^+$ which show that the transitions from the porphyrin molecular orbitals are not affected by the oxidation/reduction of the ethynylruthenium redox centre. The same conclusions apply for **4** and $[4]^+$.

The observed IR $\nu(\text{C}\equiv\text{C})$ bands from 2068 cm^{-1} for the neutral species of the ruthenium complexes **3** and **4** to



Table 5 Comparison of computed and observed B-bands (Soret bands) and lowest energy Q-bands for **1'–4'**. Computed extinction coefficients (ϵ) were obtained by a multiple value of 240 000 on the calculated oscillator strengths (f)

B band	B band	Q band	Q band
$\lambda_{\text{max}}/\text{nm} (\epsilon)$	$\lambda_{\text{max}}/\text{nm} (\epsilon)$	$\lambda_{\text{max}}/\text{nm} (\epsilon)$	$\lambda_{\text{max}}/\text{nm} (\epsilon)$
Calculated	Observed	Calculated	Observed
1' 421 (488)	425 (624)	684 (6)	649 (5)
2' 410 (724)	428 (316)	607 (6)	596 (3)
3' 431 (484)	423 (511)	685 (9)	657 (11)
4' 420 (555)	425 (524)	609 (12)	602 (20)

1910 cm^{-1} on oxidation indicate weakening of the $\text{C}\equiv\text{C}$ bonds on oxidation. The removal of an electron from the HOMO located on the ethynylruthenium unit ($\text{RuC}\equiv\text{C}$) in **3** (or **4**) would be expected to significantly weaken the $\text{C}\equiv\text{C}$ bond length (and strengthen the Ru–C bond in $\text{RuC}\equiv\text{C}$).³⁹

On second oxidations, both **3** and **4** give absorption spectra like those of **1** and **2** on first oxidations, respectively, while **3** and **4** on first reductions give similar spectra to those of **1** and **2** on first reductions. The spectra from the first oxidations on the dyads **3** and **4** resemble overlap of the neutral porphyrins **1** and **2** respectively with a $[\text{Ru}(\text{dppe})_2(\text{C}\equiv\text{CPh})\text{Cl}]^+$ monocation. The spectroelectrochemical and computational results here thus show that the porphyrin and ethynylruthenium units in **3** and **4** can be viewed as largely independent redox centres.

The observed fluorescence quantum yields decrease when the ethynylruthenium units are attached to the corresponding porphyrins (Table 1). From our spectroelectrochemical and computational data on **3** and **4** here, a plausible explanation for the fluorescence yield decrease is the intramolecular electron transfer taking place after excitation of the complexes **3** and **4**. The porphyrins **1** and **2** emit local fluorescence after light excitation (Fig. 12). The ruthenium complex **3** (or **4**) is also initially excited at the porphyrin units but, while local porphyrin fluorescence of the complex is observed based on a similar emission spectrum (Fig. 3) to that of the corresponding porphyrin **1** (or **2**), the major pathway is the intramolecular electron transfer to a diradical excited state. The diradical, which contains a negative charge at the porphyrin unit and a positive charge at the ruthenium centre, is then returned to

the initial ground state *via* charge recombination. The latter process is non-radiative so the fluorescence quantum yields are decreased on going from **1** and **2** to **3** and **4** respectively.

Conclusions

In summary, two donor–acceptor dyads (**3** and **4**) featuring the redox-active and electron-rich $\text{Ru}(\text{dppe})_2\text{Cl}$ group as the donor site and a trifluorenylphenyl porphyrin as the acceptor site have been synthesised and characterised. The absorption and emission properties of these new compounds show that, while the precursors **1** and **2** are brighter fluorophores than H_2TPP , both **3** and **4** are much poorer fluorophores than ZnTPP . Nevertheless, **3** has a higher fluorescence quantum yield than ZnTRuEP and other related chromophores containing $\text{Ru}(\text{II})$ and $\text{Fe}(\text{II})$ acetylides complexes at their periphery such as **A** or **B** (Chart 1), reflecting the desired effect of the 2-fluorenyl groups appended to the porphyrin ring on the fluorescence. Furthermore, compounds featuring free bases are much better luminophores than compounds made of $\text{Zn}(\text{II})$ -complexed porphyrins ($\Phi_F(\mathbf{1}) > \Phi_F(\mathbf{2})$ and $\Phi_F(\mathbf{3}) > \Phi_F(\mathbf{4})$).

Electrochemical (CV) and spectroelectrochemical studies on **1–4** show at least two kinetically stable redox states present. Compounds **1** and **3** featuring free base porphyrins have much better redox stabilities than compounds **2** and **4** with $\text{Zn}(\text{II})$ -complexed porphyrins. The nature of the first excited states of these derivatives in their mono-oxidised, di-oxidised and mono-reduced states are interpreted on the basis of computed electronic structures on optimised geometries of **1–4**. For **3**, there is the possibility for achieving a strong modulation of the cubic (and even quadratic) NLO properties at carefully selected wavelengths by reduction. In contrast, a much poorer modulation of the NLO properties is expected upon oxidation for **3** and **4** based on these studies. Controlling the luminescence of these derivatives, in particular for compounds **1** and **3** where three and four stable redox states respectively are accessible, by redox-switching appears promising. Current work on this aspect is underway.

Experimental section

General procedures

All reaction mixtures were performed under argon and were magnetically stirred. Solvents were distilled from appropriate drying agent prior to use, DCM from CaH_2 and THF from sodium/benzophenone. Other solvents used were of HPLC grade. Commercially available reagents were used without further purification unless otherwise stated.

^1H NMR and ^{13}C NMR in CDCl_3 were recorded using Bruker 200 DPX, 300 DPX and 500 DPX spectrometers. The chemical shifts were referenced to 7.26 ppm for ^1H , 77.2 ppm for ^{13}C and external H_3PO_4 at 0.0 ppm for ^{31}P . Peak assignments were performed by 2D NMR experiments where possible: COSY (Correlation Spectroscopy), HMBC (Heteronuclear

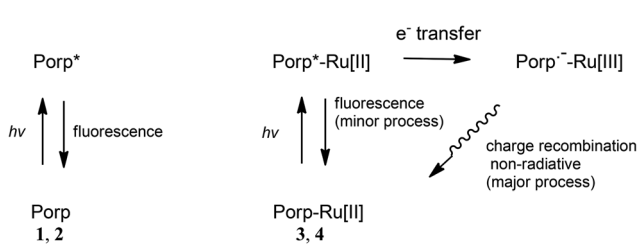


Fig. 12 Proposed photophysical processes of the porphyrins **1** and **2** (Porp) and the porphyrin–ruthenium complexes **3** and **4** (Porp-Ru[III]).



Multiple Bond Correlation) and HMQC (Heteronuclear Multiple Quantum Coherence). UV spectra were recorded on a UVIKON XL spectrometer from Biotek instruments. PL emission spectra were recorded on a Photon Technology International (PTI) apparatus coupled on an 814 Photomultiplier Detection System, Lamp Power Supply 220B and MD-5020.

Steady-state fluorescence measurements were performed at room temperature on dilute solutions (*ca.* 10⁻⁶ M) using an Edinburgh Instruments (FLS 920) spectrometer working in photon-counting mode, equipped with a calibrated quantum counter for excitation correction. The dichloromethane solutions used were 10 times more concentrated for the zinc complex **4** (~10⁻⁶ M) than for the free base **3** (~10⁻⁵ M). Fluorescence quantum yields were measured using standard methods; **H₂TPP** in DCM (Φ_f = 0.12 at λ_{ex} = 417 nm) was used as a reference. The estimated uncertainty on the reported fluorescence quantum yields is $\pm 10\%$.

Additional characterisation data; **1** FT-IR (KBr disc, cm⁻¹): 3306 (w, NH stretch), 3272 (w, C≡C-H stretch), 3037 (s, aromatic CH stretch), 2920 (w, aliphatic CH stretch), 2104 (w, C≡C stretch); ¹³C{¹H} NMR (400 MHz, CDCl₃, δ in ppm): 143.9, 141.9, 141.7, 141.4, 140.8, 134.7, 133.7, 131.6 (CH in C₆H₄), 131.5, 130.8, 130.7 (CH in C₆H₄), 127.3, 125.5, 121.8, 121.0, 120.9, 120.5, 119.1, 118.2, 78.5 (C≡CH), 37.3 (fluorenyl CH₂). **2** FT-IR (KBr disc, cm⁻¹): 3294 (w, C≡C-H stretch), 3053 (s, aromatic CH stretch), 2920 (w, aliphatic CH stretch), 2108 (w, C≡C stretch); ¹³C{¹H} NMR (400 MHz, CDCl₃, δ in ppm): 150.7, 150.6, 150.0, 143.9, 143.7, 141.8, 141.4, 141.2, 137.6, 134.5, 133.6, 132.4, 132.3, 131.8 (CH in C₆H₄), 131.5, 130.6 (CH in C₆H₄), 127.2, 125.4, 122.0, 121.8, 121.5, 120.4, 120.12, 118.0, 78.3 (C≡CH), 37.3 (fluorenyl CH₂).

Synthesis of 5,10,15-(trifluorenyl)-20-(4-ethynyl-ruthenium-phenyl)porphyrin 3. A solution of **1** (0.045 g, 0.050 mmol) and [Ru(dppe)₂Cl][PF₆] (0.06 g, 0.055 mmol), in distilled DCM (18 mL) was stirred in a Schlenk tube at ambient temperature under argon. The reaction mixture was monitored by ³¹P and ¹H NMR spectroscopy and was judged to be completed in 72 hours. The reaction mixture was concentrated under reduced pressure and adding ether to the mixture gave a precipitate containing the desired vinylidene. The solid was filtered, dissolved in 10 mL of DCM and triethylamine was added dropwise (0.25 mL). The brown-green solution was concentrated, filtered through a short basic alumina column using DCM and 2% triethylamine as eluent. The solution was concentrated and addition of ether to the solution gave a greenish-brown solid **3** (20 mg, 22% yield). ¹H NMR (400 MHz, CDCl₃, δ in ppm): 9.01 (d, 2H, $^3J_{HH}$ = 4.8 Hz, H_β-pyrrolic), 8.97 (d, 2H, $^3J_{HH}$ = 4.8 Hz, H_β-pyrrolic), 8.93 (s, 4H, H_β-pyrrolic), 8.41 (m, 3H, H_{fluorenyl}, H₁), 8.28 (m, 3H, H_{fluorenyl}, H₄), 8.16 (m, 3H, H_{fluorenyl}, H₃), 8.06 (d, 3H, $^3J_{HH}$ = 7.2 Hz, H_{fluorenyl}, H₅), 7.98 (d, 2H, $^3J_{HH}$ = 8.0 Hz, H_{phenylene}), 7.72 (m, 11H, H_{fluorenyl}, H₈ and *ortho* H_{PPh}), 7.53 (m, 3H, H_{fluorenyl}, H₆), 7.44 (m, 3H, H_{fluorenyl}, H₇), 7.33 (m, 8H, *ortho* H_{PPh}), 7.27 (t, 4H, $^3J_{HH}$ = 7.2 Hz, *para* H_{PPh}), 7.22 (t, 4H, $^3J_{HH}$ = 7.2 Hz, *para* H_{PPh}), 7.12 (t, 8H, $^3J_{HH}$ ~ 7.6 Hz, *meta* H_{PPh}), 7.04 (m, 10H, $^3J_{HH}$ ~ 7.6 Hz, *meta* H_{PPh} and H_{phenylene}), 4.22 (s, 4H, 2CH₂-fluorenyl), 4.21 (s, 2H, 1CH₂-fluorenyl), 2.80 (m, 8H, CH₂/dppe). ¹³C{¹H} NMR: 150.7, 150.5, 150.4, 143.9, 143.7, 141.8, 141.7, 141.2, 137.0 (m, *ipso* PPh), 135.8 (m, *ipso* PPh), 134.6 (*ortho* PPh), 134.3, 133.6, 132.4, 132.1, 132.0, 131.5, 129.7 (CH in C₆H₄), 129.2 (*para* PPh), 129.0 (*para* PPh), 128.3 (CH in C₆H₄), 127.5 (*meta* PPh), 127.2 (*meta* PPh), 125.5, 121.5, 120.4, 118.0, 37.3 (fluorenyl CH₂), 30.9 (dppe CH₂). ³¹P NMR (81 MHz, CDCl₃, δ in ppm): 49.7 (s). MS (ESI in CH₂Cl₂/CH₃CN): calcd for C₁₁₉H₈₇ClN₄P₄ZnRu: 1898.3923 [M]⁺, found: 1898.3932 [M]⁺. Elemental analysis: calcd for C₁₁₉H₈₇ClN₄P₄ZnRu·0.5CHCl₃: C, 73.29, H, 4.50, N, 2.86, found: C, 73.88, H, 4.54, N, 2.92. UV-vis (λ max, (ϵ , 10⁻³ M⁻¹ cm⁻¹), DCM, nm): 264 (107), 425 (524), 557 (26.6), 602 (20.4). FT-IR (KBr disc, cm⁻¹): 3050 (s, aromatic

1CH₂-fluorenyl), 2.79 (m, 8H, CH₂/dppe), -2.57 (s, 2H, NH). ¹³C{¹H} NMR: 144.0, 141.9, 141.8, 141.4, 141.1, 136.5 (m, *ipso* PPh), 135.8 (m, *ipso* PPh), 134.6 (*ortho* PPh), 133.7, 131.6, 131.1, 129.2 (*para* PPh), 129.0 (*para* PPh), 128.8 (CH in C₆H₄), 128.4 (CH in C₆H₄), 127.5 (*meta* PPh), 127.3, 127.2 (*meta* PPh), 125.5, 122.4, 120.5, 37.4 (fluorenyl CH₂), 31.0 (dppe CH₂). ³¹P NMR (81 MHz, CDCl₃, δ in ppm): 50.0 (s). MS (ESI in CH₂Cl₂/CH₃CN): calcd for C₁₁₉H₈₉ClN₄P₄Ru: 1835.4 [MH]⁺, found 1835.5 [MH]⁺; 1800.0 [M - Cl + H]⁺, found 1799.5 [M - Cl + H]⁺. MALDI-TOF MS: calcd for C₁₁₉H₈₉ClN₄P₄Ru: 1835.4 [MH]⁺, found 1835.5 [MH]⁺. Elemental Analysis: calcd for C₁₁₉H₈₉ClN₄P₄Ru: C, 77.87, H, 4.89, N, 3.05, found: C, 77.31, H, 4.98, N, 2.96. UV-vis (λ max, (ϵ , 10⁻³ M⁻¹ cm⁻¹), DCM, nm): 263 (105), 423 (511), 520 (21), 568 (18), 590 (15), 657 (11). FT-IR (KBr disc, cm⁻¹): 3310 (w, NH stretch), 3050 (s, aromatic CH stretch), 2915 (w, aliphatic CH stretch), 2058 (s, C≡C stretch).

Synthesis of Zn(*ii*)-5,10,15-(trifluorenyl)-20-(4-ethynyl-ruthenium-phenyl)porphyrinato 4. In a Schlenk tube, a solution of **2** (0.040 g, 0.041 mmol) and [Ru(dppe)₂Cl][PF₆] (0.050 g, 0.046 mmol), in distilled DCM (20 mL) was stirred under argon. The mixture was monitored by ³¹P and ¹H NMR spectroscopy, and the reaction was complete in 72 hours. The solution was concentrated under reduced pressure and adding ether gave the desired vinylidene as the precipitated solid. The unreacted ruthenium salt remained in ether. The precipitate was filtered, dissolved in 10 mL of DCM and triethylamine (0.25 mL) was added dropwise to the solution. The brown green solution was then concentrated and passed through a short basic alumina column using DCM and 2% triethylamine as eluent. The solution was concentrated and addition of ether gave a greenish brown precipitate which was filtered and identified as **4**. (19 mg, 25% yield). ¹H NMR (400 MHz, CDCl₃, δ in ppm): 9.12 (d, 2H, $^3J_{HH}$ = 4.8 Hz, H_β-pyrrolic), 9.08 (d, 2H, $^3J_{HH}$ = 4.8 Hz, H_β-pyrrolic), 9.03 (s, 4H, H_β-pyrrolic), 8.41 (m, 3H, H_{fluorenyl}, H₁), 8.28 (m, 3H, H_{fluorenyl}, H₄), 8.16 (m, 3H, H_{fluorenyl}, H₃), 8.06 (d, 3H, $^3J_{HH}$ = 7.2 Hz, H_{fluorenyl}, H₅), 7.98 (d, 2H, $^3J_{HH}$ = 8.0 Hz, H_{phenylene}), 7.72 (m, 11H, H_{fluorenyl}, H₈ and *ortho* H_{PPh}), 7.53 (m, 3H, H_{fluorenyl}, H₆), 7.44 (m, 3H, H_{fluorenyl}, H₇), 7.33 (m, 8H, *ortho* H_{PPh}), 7.27 (t, 4H, $^3J_{HH}$ = 7.2 Hz, *para* H_{PPh}), 7.22 (t, 4H, $^3J_{HH}$ = 7.2 Hz, *para* H_{PPh}), 7.12 (t, 8H, $^3J_{HH}$ ~ 7.6 Hz, *meta* H_{PPh}), 7.04 (m, 10H, $^3J_{HH}$ ~ 7.6 Hz, *meta* H_{PPh} and H_{phenylene}), 4.22 (s, 4H, 2CH₂-fluorenyl), 4.21 (s, 2H, 1CH₂-fluorenyl), 2.80 (m, 8H, CH₂/dppe). ¹³C{¹H} NMR: 150.7, 150.5, 150.4, 143.9, 143.7, 141.8, 141.7, 141.2, 137.0 (m, *ipso* PPh), 135.8 (m, *ipso* PPh), 134.6 (*ortho* PPh), 134.3, 133.6, 132.4, 132.1, 132.0, 131.5, 129.7 (CH in C₆H₄), 129.2 (*para* PPh), 129.0 (*para* PPh), 128.3 (CH in C₆H₄), 127.5 (*meta* PPh), 127.2 (*meta* PPh), 125.5, 121.5, 120.4, 118.0, 37.3 (fluorenyl CH₂), 30.9 (dppe CH₂). ³¹P NMR (81 MHz, CDCl₃, δ in ppm): 49.7 (s). MS (ESI in CH₂Cl₂/CH₃CN): calcd for C₁₁₉H₈₇ClN₄P₄ZnRu: 1898.3923 [M]⁺, found: 1898.3932 [M]⁺. Elemental analysis: calcd for C₁₁₉H₈₇ClN₄P₄ZnRu·0.5CHCl₃: C, 73.29, H, 4.50, N, 2.86, found: C, 73.88, H, 4.54, N, 2.92. UV-vis (λ max, (ϵ , 10⁻³ M⁻¹ cm⁻¹), DCM, nm): 264 (107), 425 (524), 557 (26.6), 602 (20.4). FT-IR (KBr disc, cm⁻¹): 3050 (s, aromatic



CH stretch), 2914 (w, aliphatic CH stretch), 2058 (s, C≡C stretch).

Electrochemistry

Cyclic voltammograms were recorded with an Autolab PG-STAT 30 potentiostat at 20 °C from solutions of *ca.* 10⁻⁴ M analyte in dry DCM containing 0.1 M tetra-*n*-butylammonium hexafluorophosphate [Bu₄N][PF₆] at scan rate $\nu = 100$ mV s⁻¹ under a dry nitrogen atmosphere. The single-compartment three-electrode cell was equipped with platinum wire counter and reference electrodes and a glassy carbon working electrode. All redox potentials are reported with the decamethylferrocene/decamethylferrocenium (Cp²Fe⁺/Cp²Fe) redox couple used as an internal reference system at -0.53 V (ref. 27) *vs.* the usual ferrocene/ferrocenium (Cp₂Fe⁺/Cp₂Fe) redox couple at 0.0 V in DCM.

Spectroelectrochemistry

Spectroelectrochemical (SEC) experiments were performed at room temperature in an airtight optically transparent thin-layer electrochemical (OTTLE) cell⁴⁰ equipped with Pt minigrid working and counter electrodes (32 wires cm⁻¹), Ag wire pseudo-reference electrode and CaF₂ windows for a 200 μ m path-length solvent compartment. DCM solutions containing 0.1 M [Bu₄N][PF₆] electrolyte were used in the cell for SEC experiments. The cell was fitted into the sample compartment of a Cary UV-Vis-IR spectrophotometer or a Nicolet Avatar 6700 FT-IR spectrometer. Bulk electrolysis was carried out using an Autolab PG-STAT 30 potentiostat.

Computations

All computations were carried out with the Gaussian 09 package.⁴¹ The four model S₀ geometries 1'-4' with no symmetry constraints were fully optimised with the B3LYP functional⁴² using the 3-21G* basis set⁴³ for all atoms. The 3-21G* basis set is used here as it has been shown to be suitable for ruthenium acetylides elsewhere.^{34,39,44} Frequency calculations on these geometries revealed no imaginary frequencies. Computed absorption data were obtained from TD-DFT⁴⁵ calculations on S₀ geometries using the CAM-B3LYP functional.⁴⁶ As the CAM-B3LYP functional generally overestimates the transition energies, compared to that of experimental and B3LYP data, a scaling factor of 0.85 was applied.⁴⁷ The MO diagrams were generated with the Gabedit package⁴⁸ and the %MO contributions were obtained using the GaussSum software.⁴⁹

Acknowledgements

We thank "Région Bretagne" (ARED; A.M.), China Scholarship Council (CSC; D. Y. and X. Z.), MENRT (S.D.) and EPSRC (J.A. G.W. and M.A.F.) for funding. We also thank CNRS and Durham University for supporting the Rennes-Durham collaboration.

References

- See for example: (a) P. Gautam, B. Dhokale, V. Shukla, C. P. Singh, K. S. Bindra and R. Misra, *J. Photochem. Photobiol. A*, 2012, **239**, 24–27; (b) V. N. Nemykin and R. G. Hadt, *J. Phys. Chem. A*, 2010, **114**, 12062–12066; (c) F. D'Souza, P. M. Smith, S. Gadde, A. L. McCarty, M. J. Kullman, M. E. Zandler, M. Itou, Y. Araki and O. Ito, *J. Phys. Chem. B*, 2004, **108**, 11333–11343; (d) Q. Li, G. Mathur, G. Gowda, S. Surthi, Q. Zhao, L. Yu, J. S. Lindsey, D. F. Bocian and V. Misra, *Adv. Mater.*, 2004, **16**, 133–137.
- S. di Bella, C. Dragonetti, M. Pizzotti, D. Roberto, F. Tessore and R. Ugo, *Top. Organomet. Chem.*, 2010, **28**, 1–55.
- C. Bucher, C. H. Devillers, J.-C. Moutet, G. Royal and E. Saint-Aman, *Coord. Chem. Rev.*, 2009, **253**, 21–36.
- G. Grelaud, M. P. Cifuentes, F. Paul and M. G. Humphrey, *J. Organomet. Chem.*, 2014, **751**, 181–200.
- S. Drouet, A. Merhi, G. Grelaud, M. P. Cifuentes, M. G. Humphrey, K. Matczyszyn, M. Samoc, L. Toupet, C. O. Paul-Roth and F. Paul, *New J. Chem.*, 2012, **36**, 2192–2195.
- S. Drouet, A. Merhi, D. Yao, M. P. Cifuentes, M. G. Humphrey, M. Wielgus, J. Olesiak-Banska, K. Matczyszyn, M. Samoc, F. Paul and C. O. Paul-Roth, *Tetrahedron*, 2012, **68**, 10351–10359.
- A. Merhi, G. Grelaud, N. Ripoche, A. Barlow, M. P. Cifuentes, M. G. Humphrey, F. Paul and C. O. Paul-Roth, *Polyhedron*, 2015, **86**, 64–70.
- M. Murai, M. Sugimoto and M. Akita, *Dalton Trans.*, 2013, **42**, 16108–16120.
- J. Rochford, A. D. Rooney and M. T. Pryce, *Inorg. Chem.*, 2007, **46**, 7247–7249.
- There are many NLO switching compounds reported in the literature (usually with ferrocenyl group as the redox-switching group): (a) K. L. Kott, D. A. Higgins, R. J. McMahon and M. Corn, *J. Am. Chem. Soc.*, 1993, **115**, 5342–5343; (b) T. Kondo, S. Horiuchi, I. Yagi, S. Ye and K. Uosaki, *J. Am. Chem. Soc.*, 1999, **121**, 391–398; (c) M. Malaun, Z. R. Reeves, R. L. Paul, J. C. Jeffery, J. A. MacCleverty, M. D. Ward, I. Asselberghs, K. Clays and A. Persoons, *Chem. Commun.*, 2001, 49–50; (d) C. Sporer, I. Ratera, D. Ruiz-Molina, Y. Zhao, J. Vidal-Gancedo, K. Wurst, P. Jaitner, K. Clays, A. Persoons, C. Rovira and J. Veciana, *Angew. Chem., Int. Ed.*, 2004, **43**, 5266–5268; (e) L. Boubekeur-Lecaque, B. J. Coe, K. Clays, S. Foerier, T. Verbiest and I. Asselberghs, *J. Am. Chem. Soc.*, 2008, **130**, 3286–3287; (f) W.-Y. Wang, N.-N. Ma, S.-L. Sun and Y.-Q. Qiu, *Organometallics*, 2014, **33**, 3341–3352; (g) B. J. Coe, S. Houbrechts, I. Asselberghs and A. Persoons, *Angew. Chem., Int. Ed.*, 1999, **38**, 366–368; (h) I. Asselberghs, K. Clays, A. Persoons, M. D. Ward and J. MacCleverty, *J. Mater. Chem.*, 2004, **14**, 2831–2839; (i) I. Asselberghs, K. Clays, A. Persoons, M. D. Ward and J. MacCleverty, *J. Mater. Chem.*, 2004, **14**, 2831–2839; (j) B. J. Coe, *Acc. Chem. Res.*, 2006, **39**, 383–393.

11 K. A. Green, M. P. Cifuentes, M. Samoc and M. G. Humphrey, *Coord. Chem. Rev.*, 2011, **255**, 2530–2541.

12 (a) K. M.-C. Wong, S. C.-F. Lam, C.-C. Ko, N. Zhu, V. W.-W. Yam, S. Roué, C. Lapinte, S. Fathallah, K. Costuas, S. Kahlal and J.-F. Halet, *Inorg. Chem.*, 2003, **42**, 7086–7097; (b) L. Norel, E. Di Piazza, M. Feng, A. Vacher, X. He, T. Roisnel, O. Maury and S. Rigaut, *Organometallics*, 2014, **33**, 4824–4835; (c) E. Di Piazza, L. Norel, K. Costuas, A. Bourdolle, O. Maury and S. Rigaut, *J. Am. Chem. Soc.*, 2011, **133**, 6174–6775; (d) M. Tropiano, N. L. Kilah, M. Morten, H. Rahman, J. J. Davis, P. D. Beer and S. Faulkner, *J. Am. Chem. Soc.*, 2011, **133**, 11847–11849; (e) M. Yano, K. Matsuhiro, M. Tatsumi, Y. Kashiwagi, M. Nakamoto, M. Oyama, K. Ohkubo, S. Fukuzumi, H. Misaki and H. Tsukube, *Chem. Commun.*, 2012, **48**, 4082–4084; (f) T. Sato and M. Higuchi, *Chem. Commun.*, 2013, **49**, 5256–5259.

13 P. Audebert and F. Miomandre, *Chem. Sci.*, 2013, **4**, 575–584.

14 C. Paul-Roth, J. A. G. Williams, J. Letessier and G. Simonneaux, *Tetrahedron Lett.*, 2007, **48**, 4317–4322.

15 C. O. Paul-Roth and G. Simonneaux, *Tetrahedron Lett.*, 2006, **47**, 3275–3278.

16 C. O. Paul-Roth and G. Simonneaux, *C. R. Acad. Sci., Ser. IIb: Mec., Phys., Astron.*, 2006, **9**, 1277–1286.

17 For recent examples of Ru(dppe)₂Cl-acetylides, see: (a) G. Grelaud, M. P. Cifuentes, T. Schwich, G. Argouarch, S. Petrie, R. Strange, F. Paul and M. G. Humphrey, *Eur. J. Inorg. Chem.*, 2012, **1**, 65–75; (b) P. J. West, T. Schwich, M. P. Cifuentes and M. G. Humphrey, *J. Organomet. Chem.*, 2011, **696**, 2886–2893; (c) Y. Liu, C. M. Ndiaye, C. Lagrost, K. Costuas, S. Choua, P. Turek, L. Norel and S. Rigaut, *Inorg. Chem.*, 2014, **53**, 8172–8188; (d) S. Marqués-González, M. Parthey, D. S. Yufit, J. A. K. Howard, M. Kaupp and P. J. Low, *Organometallics*, 2014, **33**, 4947–4963; (e) M. Parthey, J. B. G. Gluyas, M. A. Fox, P. J. Low and M. Kaupp, *Chem. – Eur. J.*, 2014, **20**, 6895–6908; (f) S. S. Chavan and B. G. Bharate, *Inorg. Chim. Acta*, 2013, **394**, 598–604; (g) R. Gatri, I. Ouerfelli, M. L. Efrit, F. Serein-Spirau, J.-P. Lère-Porte, P. Valvin, T. Roisnel, S. Bivaud, H. Akdas-King and J.-L. Fillaut, *Organometallics*, 2014, **33**, 665–676; (h) M. I. Bruce, M. L. Cole, K. Costuas, B. G. Ellis, K. A. Kramarczuk, C. Lapinte, B. K. Nicholson, G. J. Perkins, B. W. Skelton, A. H. White and N. N. Zaitseva, *Z. Anorg. Allg. Chem.*, 2013, **639**, 2216–2223.

18 A. Merhi, S. Drouet, N. Kerisit and C. O. Paul-Roth, *Tetrahedron*, 2013, **69**, 7112–7124.

19 C. O. Paul-Roth, A. Merhi, D. Yao and O. Mongin, *J. Photochem. Photobiol. A*, 2014, **288**, 23–33.

20 S. Guesmi, D. Touchard and P. H. Dixneuf, *Chem. Commun.*, 1996, 2773–2774.

21 D. Touchard, C. Morice, V. Cadiero, P. Haquette, L. Toupet and P. H. Dixneuf, *J. Chem. Soc., Chem. Commun.*, 1994, 859–860.

22 J. W. Owens, R. Smith, R. Robinson and M. Robins, *Inorg. Chim. Acta*, 1998, **279**, 226–231.

23 S. Drouet and C. O. Paul-Roth, *Tetrahedron*, 2009, **65**, 10693–10700.

24 S. Drouet, A. Merhi, G. Argouarch, F. Paul, O. Mongin, M. Blanchard-Desce and C. O. Paul-Roth, *Tetrahedron*, 2012, **68**, 98–105.

25 C. Paul-Roth, J. Rault-Berthelot, G. Simonneaux, C. Poriel, M. Abdalilah and J. Letessier, *J. Electroanal. Chem.*, 2006, **597**, 19–27.

26 C. Paul-Roth, J. Rault-Berthelot, G. Simonneaux, J. Letessier and J.-F. Bergamini, *J. Electroanal. Chem.*, 2007, **606**, 103–116.

27 M. A. Fox, J. E. Harris, S. Heider, V. Pérez-Gregorio, M. E. Zakrzewska, J. D. Farmer, D. S. Yufit, J. A. K. Howard and P. J. Low, *J. Organomet. Chem.*, 2009, **694**, 2350–2358.

28 M. V. Sheridan, K. Lam and W. E. Geiger, *Angew. Chem., Int. Ed.*, 2013, **52**, 12897–12900.

29 C. E. Powell, M. P. Cifuentes, J. P. Morrall, R. Stranger, M. G. Humphrey, M. Samoc, B. Luther-Davies and G. A. Heath, *J. Am. Chem. Soc.*, 2003, **125**, 602–610.

30 N. Gauthier, N. Tchouar, F. Justaud, G. Argouarch, M. P. Cifuentes, L. Toupet, D. Touchard, J.-F. Halet, S. Rigaut, M. G. Humphrey, K. Costuas and F. Paul, *Organometallics*, 2009, **28**, 2253–2266.

31 G. Peychal-Heiling and G. S. Wilson, *Anal. Chem.*, 1971, **43**, 550–556.

32 C. Paliteiro and A. Sobral, *Electrochim. Acta*, 2005, **50**, 2445–2451.

33 J. Fajer, D. C. Borg, A. Forman, D. Dolphin and R. H. Felton, *J. Am. Chem. Soc.*, 1970, **92**, 3451–3459.

34 M. A. Fox, J. D. Farmer, R. L. Roberts, M. G. Humphrey and P. J. Low, *Organometallics*, 2009, **28**, 5266–5269.

35 M. Gouterman, *J. Mol. Spectrosc.*, 1961, **6**, 138–163.

36 C.-K. Tai, W.-H. Chuang and B.-C. Wang, *J. Lumin.*, 2013, **142**, 8–16.

37 L. Weber, D. Eickhoff, T. B. Marder, M. A. Fox, P. J. Low, A. D. Dwyer, D. J. Tozer, S. Schwedler, A. Brockhinke, H.-G. Stammler and B. Neumann, *Chem. – Eur. J.*, 2012, **18**, 1369–1382.

38 E. A. Alemán, J. M. Rocha, W. Wongwitwichote, L. A. G. Mora-Tovar and D. A. Modarelli, *J. Phys. Chem. A*, 2011, **115**, 6456–6471.

39 M. A. Fox, R. L. Roberts, W. M. Khairul, F. Hartl and P. J. Low, *J. Organomet. Chem.*, 2007, **692**, 3277–3290.

40 M. Krejcik, M. Danek and F. Hartl, *J. Electroanal. Chem.*, 1991, **317**, 179–187.

41 M. J. Frisch, G. W. Trucks, H. B. Schlegel, G. E. Scuseria, M. A. Robb, J. R. Cheeseman, G. Scalmani, V. Barone, B. Mennucci, G. A. Petersson, H. Nakatsuji, M. Caricato, X. Li, H. P. Hratchian, A. F. Izmaylov, J. Bloino, G. Zheng, J. L. Sonnenberg, M. Hada, M. Ehara, K. Toyota, R. Fukuda, J. Hasegawa, M. Ishida, T. Nakajima, Y. Honda, O. Kitao, H. Nakai, T. Vreven Jr., J. A. Montgomery, J. E. Peralta, F. Ogliaro, M. Bearpark, J. J. Heyd, E. Brothers, K. N. Kudin, V. N. Staroverov, R. Kobayashi, J. Normand,



K. Raghavachari, A. Rendell, J. C. Burant, S. S. Iyengar, J. Tomasi, M. Cossi, N. Rega, J. M. Millam, M. Klene, J. E. Knox, J. B. Cross, V. Bakken, C. Adamo, J. Jaramillo, R. Gomperts, R. E. Stratmann, O. Yazyev, A. J. Austin, R. Cammi, C. Pomelli, J. W. Ochterski, R. L. Martin, K. Morokuma, V. G. Zakrzewski, G. A. Voth, P. Salvador, J. J. Dannenberg, S. Dapprich, A. D. Daniels, O. Farkas, J. B. Foresman, J. V. Ortiz, J. Cioslowski and D. J. Fox, *Gaussian 09, Revision A.02*, Gaussian, Inc., Wallingford, CT, 2009.

42 (a) A. D. Becke, *J. Chem. Phys.*, 1993, **98**, 5648–5652; (b) C. Lee, W. Yang and R. G. Parr, *Phys. Rev. B: Condens. Matter*, 1988, **37**, 785–789.

43 (a) G. A. Petersson and M. A. Al-Laham, *J. Chem. Phys.*, 1991, **94**, 6081–6090; (b) G. A. Petersson, A. Bennett, T. G. Tensfeldt, M. A. Al-Laham, W. A. Shirley and J. Mantzaris, *J. Chem. Phys.*, 1988, **89**, 2193–2218.

44 (a) M.-C. Oerthel, D. S. Yufit, M. A. Fox, M. R. Bryce and P. J. Low, *Organometallics*, 2015, DOI: 10.1021/om501186c; (b) M. A. Fox, B. Le Guennic, R. L. Roberts, D. A. Brue, D. S. Yufit, J. A. K. Howard, G. Manca, J.-F. Halet, F. Hartl and P. J. Low, *J. Am. Chem. Soc.*, 2011, **133**, 18433–18446; (c) M. I. Bruce, A. Burgun, M. A. Fox, M. Jevric, P. J. Low, B. K. Nicholson, C. R. Parker, B. W. Skelton, A. H. White and N. N. Zaitseva, *Organometallics*, 2013, **32**, 3286–3299; (d) M. I. Bruce, M. A. Fox, P. J. Low, B. K. Nicholson, C. R. Parker, W. C. Patalinghug, B. W. Skelton and A. H. White, *Organometallics*, 2012, **31**, 2639–2657; (e) D. J. Armitt, M. I. Bruce, M. Gaudio, N. N. Zaitseva, B. W. Skelton, A. H. White, B. Le Guennic, J.-F. Halet, M. A. Fox, R. L. Roberts, F. Hartl and P. J. Low, *Dalton Trans.*, 2008, 6763–6775; (f) M. A. Fox, R. L. Roberts, T. E. Baines, B. Le Guennic, J.-F. Halet, F. Hartl, D. S. Yufit, D. Albesa-Jové, J. A. K. Howard and P. J. Low, *J. Am. Chem. Soc.*, 2008, **130**, 3566–3578; (g) J.-L. Xia, W. Y. Man, X. Zhu, C. Zhang, G.-J. Jin, P. A. Schauer, M. A. Fox, J. Yin, G.-A. Yu, P. J. Low and S. H. Liu, *Organometallics*, 2012, **31**, 5321–5333.

45 E. Runge and E. K. U. Gross, *Phys. Rev. Lett.*, 1984, **52**, 997–1000.

46 T. Yanai, D. P. Tew and N. C. Handy, *Chem. Phys. Lett.*, 2004, **393**, 51–57.

47 L. Weber, J. Halama, K. Hanke, L. Böhling, A. Brockhinke, H.-G. Stamm, B. Neumann and M. A. Fox, *Dalton Trans.*, 2014, **43**, 3347–3363.

48 A. R. Allouche, *J. Comput. Chem.*, 2011, **32**, 174–182.

49 N. M. O'Boyle, A. L. Tenderholt and K. M. Langner, *J. Comput. Chem.*, 2008, **29**, 839–845.

